O/N_2 changes during 1–4 October 2002 storms: IMAGE SI-13 and TIMED/GUVI observations

Y. Zhang, L. J. Paxton, D. Morrison, B. Wolven, H. Kil, and C.-I. Meng
Johns Hopkins University Applied Physics Laboratory, Laurel, Maryland, USA

S. B. Mende and T. J. Immel
Space Science Laboratory, University of California, Berkeley, California, USA

Received 16 February 2004; revised 29 July 2004; accepted 13 August 2004; published 29 October 2004.

[1] Thermospheric O/N_2 column density ratios referenced at a N_2 column density of 10^{17} cm^{-2} are obtained using the IMAGE SI-13 and TIMED/GUVI far-ultraviolet (FUV) dayglow data, AURIC simulation results, and MSIS86 model. Each of the magnetic storms occurring during a 4-day period (1–4 October 2002) caused significant O/N_2 depletion that was detected by both of the IMAGE SI-13 and GUVI instruments. The depletion extended down to latitudes of 10° and −5° in the Northern and Southern Hemispheres, respectively. Simultaneous measurements show an excellent agreement between the SI-13 and GUVI O/N_2 on both global and local scales. The IMAGE SI-13 O/N_2 data provide direct optical evidence that the O/N_2 depletion corotates with the Earth. The GUVI O/N_2 indicate the depletion in both of the hemispheres is not symmetric owing to the seasonal effect and differences in heating and convection induced winds. Both the IMAGE SI-13 and GUVI O/N_2 maps also provide a good opportunity for future modeling efforts. *INDEX TERMS:* 0310 Atmospheric Composition and Structure: Airglow and aurora; 0340 Atmospheric Composition and Structure: Middle atmosphere—composition and chemistry; 1640 Global Change: Remote sensing; 1610 Global Change: Atmosphere (0315, 0325); 2788 Magnetospheric Physics: Storms and substorms; *KEYWORDS:* thermospheric composition change, magnetic storm

Citation: Zhang, Y., L. J. Paxton, D. Morrison, B. Wolven, H. Kil, C.-I. Meng, S. B. Mende, and T. J. Immel (2004), O/N_2 changes during 1–4 October 2002 storms: IMAGE SI-13 and TIMED/GUVI observations, *J. Geophys. Res.*, *109*, A10308, doi:10.1029/2004JA010441.

1. Introduction

[2] Magnetic storms usually cause significant departures of ionospheric electron densities from their normal values. A decrease in peak electron density of the ionosphere brought about by magnetospheric storms has been measured and has attracted much interest for many decades [*Appleton and Ingram*, 1935; *Prölss*, 1980; *Schunk and Sojka*, 1996; *Prölss*, 1997; *Fuller-Rowell et al.*, 1996; *Buonsanto*, 1999]. *Seaton* [1956] first suggested that decrease of the electron density might be tied to thermospheric neutral composition. *Duncan* [1969] supported the hypothesis based on a more rigorous analysis. Much progress has been made over the decades, and the major processes that drive changes in the midlatitude and high-latitude thermospheric composition during magnetic storms can be described with some confidence.

[3] During a geomagnetic storm, intense Joule and particle heating causes strong upwelling of the atmosphere around the auroral oval. The strong upwelling of the atmosphere transports oxygen-depleted or nitrogen-rich air up from much lower in the thermosphere into the *F* region [*Mayr and Volland*, 1972; *Mayr et al.*, 1978; *Prölss*, 1980]. Neutral winds then redistribute this nitrogen-rich/oxygen-depleted air over much of the high-latitude region and part of the middle-latitude region. The nitrogen-rich/oxygen-depleted air causes a reduction in the ionospheric electron density. The transport is strongest during postmidnight hours owing to wind surges arising from ion convection and the associated momentum transfer to neutrals. With a sufficiently strong wind surge, the disturbed region extends to middle/low latitude and then corotates with the Earth. Effects of the composition change can be viewed in FUV dayglow when the composition change emerges from the nightside [*Strickland et al.*, 2001]. Many studies show that composition changes are due to an overall depletion of oxygen throughout the lower thermosphere extending up to *F* region heights with enhancements in N_2 and O_2 at higher altitudes [*Mayr and Volland*, 1972; *Hays et al.*, 1973; *Prölss et al.*, 1988; *Burns et al.*, 1989]. An oxygen depletion is required based on FUV observations while molecular enhancement is required to reproduce coincident ionospheric measurements [e.g., *Prölss and Craven*, 1998].

[4] *Craven et al.* [1994] introduced the idea that FUV dayglow from atomic oxygen, such as 130.4 nm emission, could be used to study the depletion of atomic oxygen during magnetic storms. It is utilized in subsequent investigations by *Nicholas et al.* [1997] and *Immel et al.* [1997,

0148-0227/04/2004JA010441$09.00

2000]. *Nicholas et al.* [1997] used the FUV dayglow data, dominated by the 130.4 nm emission of neutral atomic oxygen, from Dynamics Explorer 1 (DE 1) to study the effects of increased geomagnetic activity on thermospheric oxygen column density. They found deviations of −40% to +30% in 130.4 nm brightness during intervals of increased magnetic activity compared with the brightness during magnetically quiet times. The most significant decrease (−30% to −40%) is observed equatorward of the instantaneous auroral oval only after sustained periods (∼6 hours) of intense magnetic activity (average AE greater than ∼700 nT). The decrease extends from the auroral to middle latitudes (as low as ∼30 degrees N). Decreases with a smaller magnitude do not extend as far equatorward. They are associated with sustained periods of more moderate activity with a smaller average AE (300–400 nT). The spatial extent and magnitude of the decreases in the morning sector appear greater when IMF B_y is positive. In both cases, decreases are readily observed within the polar cap. Localized enhancements of +20% to +30% occur much less frequently and are detected at the middle latitudes, well equatorward of the auroral oval [*Nicholas et al.*, 1997].

[5] *Strickland et al.* [1995] did a theoretical study on the relation between FUV OI 135.6 nm and a more quantitative term, O/N_2, defined as the column density ratio of O to N_2 referenced to a fixed column density of N_2. *Strickland et al.* [2001] found a good positive (quasi-linear) correlation between the peak electron density of *F* region (N*mF*2) and O/N_2. *Evans et al.* [1995] found that the minimum O/N_2 could be more than a factor of two smaller than the undisturbed O/N_2 values.

[6] Using the same method developed by *Craven et al.* [1994] and *Nicholas et al.* [1997] and the concept of O/N_2 ratio introduced by *Strickland et al.* [1995], *Zhang et al.* [2003] reported that the IMAGE SI-13 (mainly measuring the O 135.6 nm emission) can be used to monitor the composition changes due to magnetic storms. Their results show the region with depleted SI-13 intensities extended to equator latitudes in the Northern (summer) Hemisphere.

[7] The O/N_2 changes can also be monitored by the simultaneous 135.6 nm and LBH dayglow intensity ratios. TIMED/GUVI (Global Ultraviolet Imager) simultaneously records FUV dayglow intensities in five colors (121.6 nm, 130.4 nm, 135.6 nm, N_2 LBH short (LBHS), and long (LBHL)) [*Paxton and Meng*, 1999; *Paxton et al.*, 1999; *Christensen et al.*, 2003; *Strickland et al.*, 2004]. The GUVI 135.6 nm and LBHS intensity ratios are independent of solar EUV flux. The ratios reflect the changes in the O/N_2 ratio [*Strickland et al.*, 1995, 2004]. We use both the IMAGE/SI-13 and TIMED/GUVI data to study the O/N_2 changes during multiple storms on 1–4 October 2002. While GUVI monitors local time variation of the O/N_2, the IMAGE SI-13 monitors global changes in the O/N_2. We also conduct the first quantitative comparison of the O/N_2 ratio obtained simultaneously from two independent spacecrafts. Such comparison provides more information on the O/N_2 changes and performance of the instruments.

2. Data and Method

[8] The FUV dayglow images from the IMAGE SI-13 and TIMED GUVI instruments are used to extract the atmospheric O/N_2 ratios. The IMAGE (apogee at 7 Re) SI-13 instrument detects the OI 135.6 nm emissions and provides a global image every 2 min. It has a field of view of 16 × 16 degrees. Its detector has 128 × 128 pixels. Its laboratory-calibrated sensitivity is 1.3×10^{-2} counts per Rayleigh per pixel for each 5-s viewing exposure per satellite revolution (120 s) [*Mende et al.*, 2000]. The SI-13 instrument has its peak response at 135.6 nm with a bandpass between wavelengths 131.0 and 140.0 nm, defined as its sensitivity drops to ∼1% of its peak value. As discussed in detail later, the SI-13, similar to GUVI, picks up both the 135.6 nm emissions from atomic oxygen and some contribution from the N_2 LBH emissions (in case of the SI-13 this is ∼40% of the total SI-13 intensity during magnetically quiet time). GUVI also uses a spectrographic technique, but it simultaneously provides cross-track scanned FUV images (15 s/scan, 97 min/orbit) in five "colors": the H Lyman α (121.6 nm), OI (130.4 nm), OI (135.6 nm) lines, N_2 LBHS band (140.0–150.0 nm), and N_2 LBHL band (165.0–180.0 nm). Images are generated using a microprocessor-controlled cross-track scan mirror mechanism that scans the disk beginning 60° from nadir across the disk and through the limb on the antisunward side of the satellite [*Paxton et al.*, 1992, 1999; *Christensen et al.*, 1994; *Paxton and Meng*, 1999]. Each GUVI scan provides an image covering an area 2500 km by 100 km at an altitude of 150 km. Its nadir spatial resolution is 7 km by 7 km. We use the IMAGE SI-13 and GUVI 135.6 nm and LBHS images, the MSIS86 model, and simulation results from the Atmospheric Ultraviolet Radiance Integrated Code (AURIC) [*Strickland et al.*, 1999] to estimate the O/N_2 ratios.

[9] Following the method of *Nicholas et al.* [1997], we first identify magnetically quiet days and find a number of the SI-13 images during them and then construct a table by calculating the mean SI-13 intensities at each look angle (0–90 degrees) and solar zenith angle (0–100 degrees). This provides a lookup table of the quiet time SI-13 intensities (I_quiet). The relative deviation of the SI-13 intensities during storm time can be defined as (I_storm − I_quiet)/I_quiet, where the I_storm is the storm time SI-13 intensities [*Zhang et al.*, 2003].

[10] To run the AURIC code, we need to know the band pass or response curves of the instruments. Figure 1 shows the IMAGE SI-13 and the GUVI 135.6 nm channel response curves. The GUVI 135.6 nm channel, using the spectrographic technique, has a rather flat response curve. Its band pass is narrower than that of the SI-13. Both the SI-13 and GUVI 135.6 nm channel mainly detect the O 135.6 nm and some N_2 LBH emissions (the LBH emissions contribute ∼40% and 30% in the total SI-13 and GUVI intensities, respectively, during magnetic quiet time). The effect of LBH contribution in the SI-13 and GUVI 135.6 nm channel is automatically taken into account when the equations (1) and (2) are used to obtain the O/N_2 (see next paragraph). Because the GUVI measures the intensities of the 135.6 nm and LBHS emissions simultaneously and the SI-13 just records the intensity of the 135.6 nm emissions, we used two different approaches (the GUVI 135.6 nm/LBHS intensity ratios and the SI-13 intensity deviation) to get the O/N_2 ratios.

[11] In order to get quantitative O/N_2 values, a number of AURIC simulations were performed using storm time

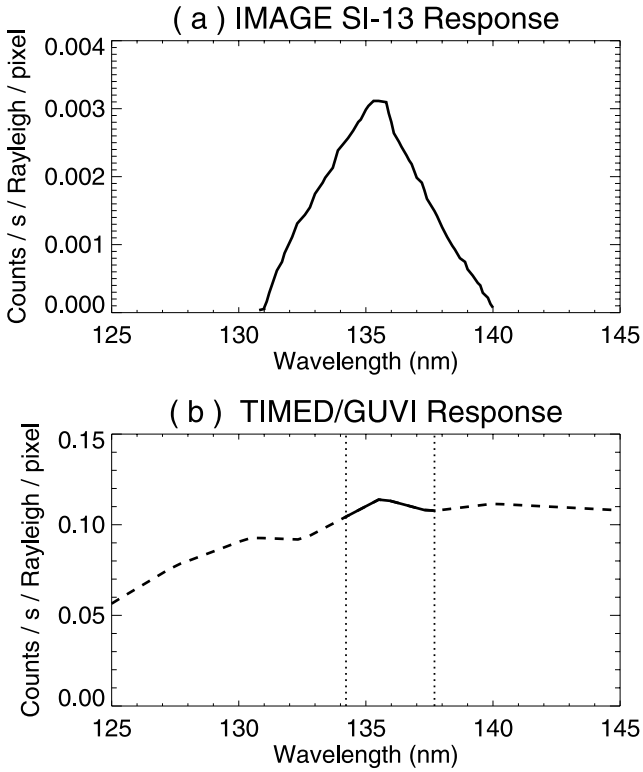

Figure 1. Response curves for (a) the IMAGE SI-13 instrument and (b) the 135.6 nm channel of the TIMED/GUVI instrument. Both of the instruments mainly measure the O 135.6 nm emission, but N_2 LBH band emissions also make some contributions.

atmospheric profiles from the MSIS86 model. A fixed solar $F10.7$ flux (150), nadir viewing geometry, and zero degrees of solar zenith angle (SZA) are assumed. Seven Ap values (164, 207, 32, 39, 22, 51, and 42) are used to drive the MSIS model. The model O/N_2 ratios are calculated from the storm time atmospheric profiles at different locations. Each AURIC run produces a spectrum between 105.0 and 900.0 nm with a wavelength resolution of 0.1 nm. The spectrum is then folded with the SI-13 response curve (considering 5-s integration time) to get the simulated SI-13 intensity in counts. Figure 2a shows the simulated SI-13 counts versus the O/N_2 column density ratio referenced at a N_2 column density level of 10^{17} cm^{-2}. The original cross section of N_2 LBH in the AUIRC code is increased owing to cascading from the a′ and w states of N_2 that is unaccounted for in the present algorithm. This causes a 60% increase in the LBH intensity [*Eastes*, 2000; *Strickland et al.*, 2004]. The solid line in Figure 2a is a minimum square fitting line that can be represented by an equation

$$\text{SI\_13\_counts} = (11.42 * O/N_2 + 7.03) \pm 0.08. \quad (1)$$

Similarly, the spectra from AURIC runs are integrated over the GUVI band passes to get simulated GUVI intensities in Rayleighs. Figure 2b shows a plot of the ratios of the simulated GUVI 135.6 nm and LBHS intensities versus the O/N_2 column density ratios. Again, the solid line in Figure 2b is a fitting line that can be represented by another equation

$$\text{GUVI 135.6 nm/LBHS Ratio} = (1.08 * O/N_2 + 0.36) \pm 0.02$$

or

$$O/N_2 = (0.926 * \text{Ratio} - 0.333) \pm 0.019. \quad (2)$$

Both of the fitting lines in Figure 2 indicate that the SI-13 counts and GUVI 135.6 nm/LBHS intensity ratios will not be zero when the O/N_2 reaches zero. This is evidence of the LBH contribution. Note that equation (2) is only valid for SZA = 0 and nadir viewing geometry of GUVI. A table from AURIC runs is used to normalize the GUVI 135.6 nm and LBHS intensities under SZA = 0 and nadir viewing condition. The normalized intensities are then applied to equation (2) to obtain the O/N_2 ratio. The equations (1)

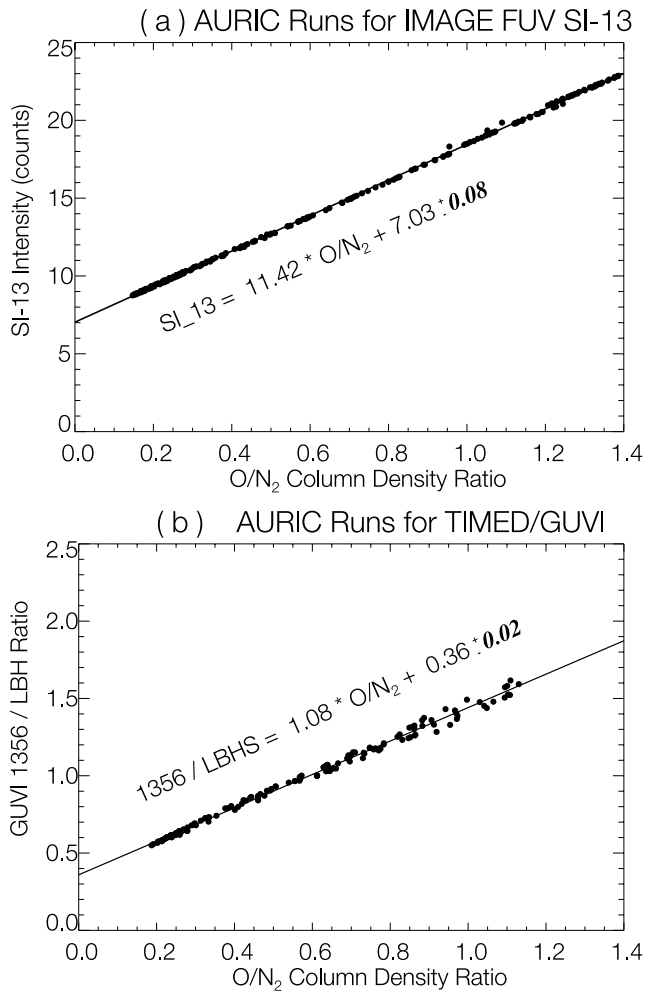

Figure 2. AURIC results (a) the simulated IMAGE SI-13 intensities and (b) the TIMED/GUVI 135.6 nm/LBHS intensity ratios versus the O/N_2 column density ratios reference at N_2 column density level of 10^{17} cm^{-2}. A fixed solar flux ($F10.7$ cm = 150) and nadir viewing geometry are used in the AURIC runs.

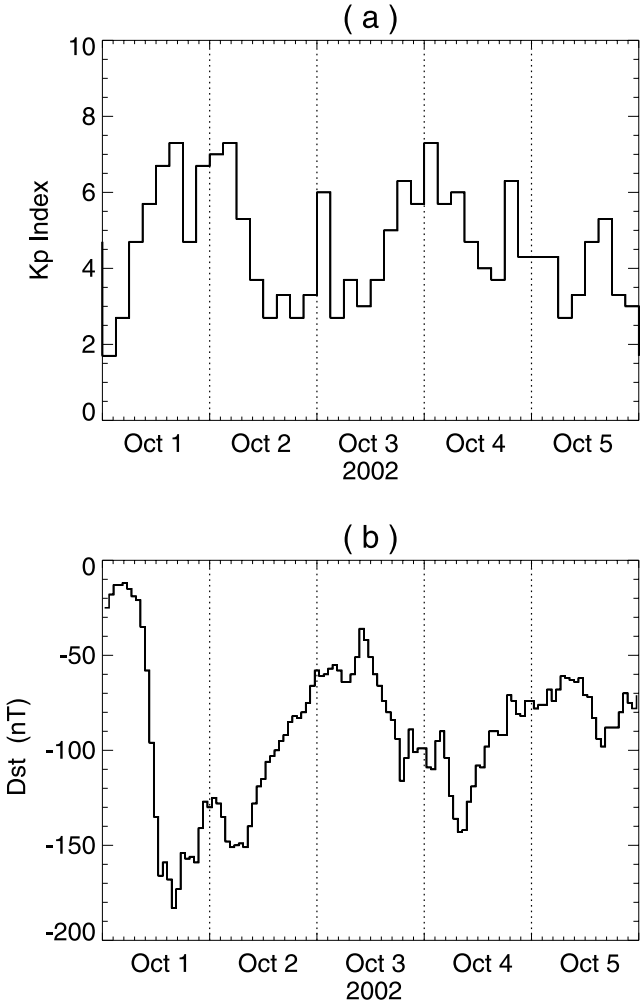

Figure 3. Plots of the (a) Kp and (b) Dst indices between 1 and 5 October 2002. The data are obtained from World Data Center 2 at Kyoto.

and (2) allow us to estimate the O/N_2 ratios from the SI-13 and GUVI data.

3. Cases During the Storms Between 1 and 4 October 2002

[12] Multimagnetic storms occurred over a period between 1 and 4 October 2002. Figure 3 shows plots of the Kp and Dst indices on 1 through 5 October 2002. The Kp index was above 6 in late 1 October, early 2 October, beginning and late 3 October, and beginning and late 4 October (see Figure 3a), indicating strong auroral activities or magnetic storms. The magnetic storms are more clearly identified by sudden decreases of the Dst index (see Figure 3b). The Kp index on 28 and 29 September (not shown here) was, however, very low (<1.7) with a daily average of 0.875 and 1.0375, respectively, indicating two magnetically quiet days.

3.1. O/N_2 Maps From the IMAGE SI-13 Images

[13] Following the same method used by *Zhang et al.* [2003], we selected the SI-13 images on 28 September to create a table of quiet time SI-13 intensities versus solar zenith angles and satellite viewing angles. The SI-13 intensity deviation is obtained as Dev = (I_storm − I_quiet)/I_quiet, where I_storm and I_quiet are the SI-13 intensities during storm and quiet time and at the same look and solar zenith angles. In order to get the absolute O/N_2 ratio, we run the MSIS86 model under a quiet condition and obtained an average O/N_2 ratio of 0.84 at latitudes between −65° and 65°. The averaged O/N_2 ratio is 0.85 over latitudes from −40 to 40 degrees, indicating the O/N_2 ratio is relatively constant at different latitudes during the quiet time. We selected 0.84 as the quiet time O/N_2 ratio. Using equation (1), we obtain the simulated quiet time SI-13 intensity (I_quiet_model = 16.62 counts). Then, the SI-13 intensity deviation form the model can be calculated by following equation:

$$\begin{aligned}\text{Deviation\_model} &= (\text{I\_model} - \text{I\_quiet\_model})/\text{I\_quiet\_model} \\ &= (11.42 * O/N_2 + 7.03 - 16.62)/16.62.\end{aligned} \tag{3}$$

Setting the deviation_model equal to the measured deviation Dev = (I_storm − I_quiet)/I_quiet, we have

$$O/N_2 = (1.456 * \text{Dev} + 0.84) \pm 0.007. \tag{4}$$

Note that the solar EUV flux (SOHO SEM data, not shown here) was nearly constant between 28 September and 2 October 2002. The solar EUV flux was ∼4% and 8% higher on 3 and 4 October 2002, respectively. The SI-13 intensities on 3 and 4 October were reduced by 4% and 8%, respectively, to compensate for the variations in the solar EUV flux, since the 135.6 nm and solar EUV emissions are linearly related [*Strickland et al.*, 1995]. Note that equation (4) is obtained for a nadir look angle and a solar zenith angle of 0 degrees. More AURIC simulations indicate that the deviation is mostly independent of the look and solar zenith angles. The error in the deviation at a large look angle (80°) and solar zenith angle (80°) is only ∼2%. Such errors are well below the statistical error (∼10%) in the SI-13 data. Thus equation (4) is not sensitive to the angles and can be used for nonnadir look and solar zenith angles. Note that the SI-13 O/N_2 in equation (4) is a function of MSIS86 climatology that is taken as truth on 28 September 2002.

[14] Figure 4 shows a selected sequence of the IMAGE SI-13 O/N_2 images between 0917 and 2356 UT on 1 October 2002. Equation (4) was used to obtain the IMAGE O/N_2 maps. Note that we estimated O/N_2 for the SI-13 pixels with solar zenith angles less than 90° only. The O/N_2 map at 0917 UT is relatively uniform with their values around 0.85, indicating a quiet time feature. This is consistent with a low Dst (between −10 and −30 nT) and low Kp values in the early hours of the day (see Figure 3). The Dst started a rapid decrease around 0930 UT and reached its minimum value of −185 nT around 1500 UT, indicating a magnetic storm. Around 1017 UT, the O/N_2 starts to show depletion in the polar cap and at the subauroral latitudes in the morningside (see Figure 4). This depletion feature was more clearly seen in the O/N_2 maps at 1218 and 1346 UT. Owing to auroral contamination, the values at the auroral oval location should

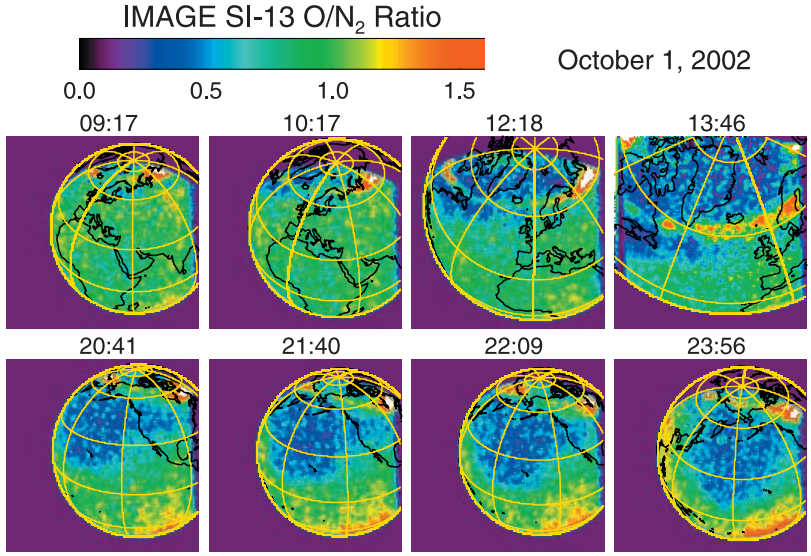

Figure 4. Selected IMAGE/SI-13 O/N_2 maps between 0917 and 2356 UT on 1 October 2002. Auroral emissions were not removed when the O/N_2 values were obtained. The effect of the auroral oval can be easily identified by high "O/N_2" values (mostly red and white in color). The maps show depleted O/N_2 in the northern polar cap and subauroral latitudes during the initial stage of a magnetic storm. The yellow circles in the maps are for latitudes at 80°, 60°, 30°, and 0° in the Northern Hemisphere. The yellow meridian lines are for longitudes from 0° (the thick line) through 360° with a 45° step size.

not be interpreted as O/N_2 ratios. With the development of the magnetic storm, the depletion region in the northern Pacific Ocean expanded into latitudes as low as 10° in the later period on 1 October 2002 (see the four O/N_2 maps in the bottom of Figure 4). Note that the expansion of the depletion is not uniform at different longitudes.

[15] The depletion region seen in Figure 4 continued to be monitored by the IMAGE SI-13 on 2 October 2002 (see the top four images between 0016 and 0314 UT, 2 October 2002 in Figure 5). The depletion region appears to remain in the Pacific Ocean. We will see that this is the evidence of corotation of the depleted region. The equatorward edge of the depleted region is shifted to a much higher latitude (~58°) in the western part of the depletion region.

[16] A weaker storm occurred early on 2 October 2002 when the Dst rapidly decreased to −150 nT around 0400 UT. This new storm caused another O/N_2 depletion (see the four images in the bottom of Figure 5). The depletion region is mainly in the eastern part of North America and the western Atlantic Ocean. Because of the weaker storm, the depletion penetrated to latitudes only slightly below 30°.

[17] It is interesting that we still see O/N_2 depletion at 0317–0758 on 3 October 2002 over Europe and western

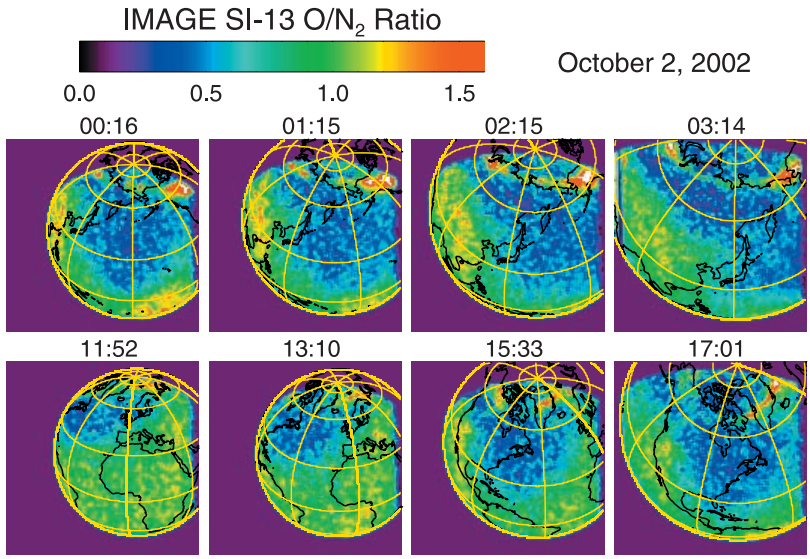

Figure 5. Similar to Figure 4, but for the IMAGE/SI-13 O/N_2 maps between 0016 and 1701 UT, 2 October 2002.

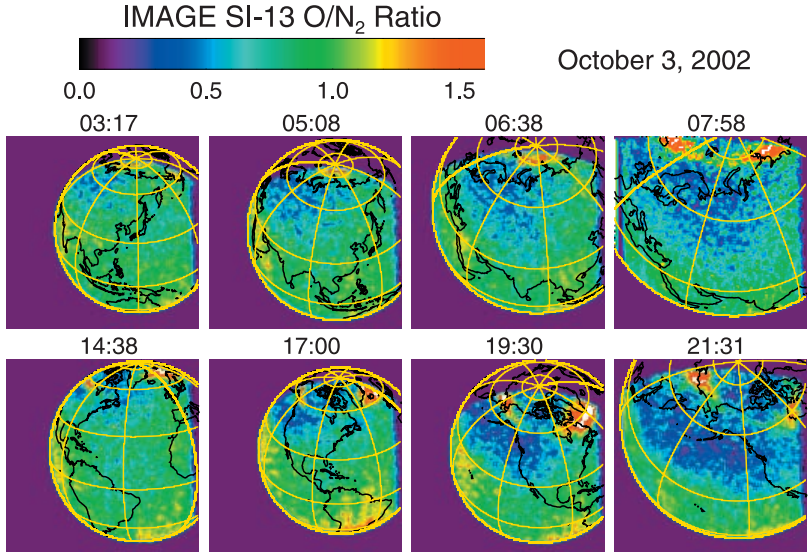

Figure 6. Similar to Figure 4, but for the IMAGE/SI-13 O/N_2 maps between 0317 and 2131 UT, 3 October 2002.

Russia (see the four images in the top of Figure 6) when the Dst recovered to −50 nT. However, the Kp suddenly reached 6 between 0000 and 0300 UT on the day (see Figure 3), indicating a magnetic storm. This is associated with a short duration of southward IMF (seen from the Wind IMF data, not shown here). Because of the short duration of southward IMF, the total heating (Joule and particle) in the nightside auroral oval may not be intense, and thus the depletion extends only to a midlatitude around 45°. Furthermore, the edges of the depletion region are more gradual than those of earlier cases that had sharp edges.

[18] A continuing slow decrease of Dst and steady increase of Kp index between 1000 and 2000 UT on 3 October 2002 (Figure 3) indicate gradually enhanced auroral activities probably with a moderate magnetic storm. GUVI auroral images (not shown here) indicate moderately enhanced auroral intensities with the auroral equatorward boundary around 60° ± 3° Mlat. The O/N_2 depletion was also observed later on 3 October 2002 (see the images in the bottom of Figure 6). The equatorward edge of the depletion region at 1930 and 2131 UT is relatively uniform around latitude of 37° (35°–40°). This is consistent with a recent study that during moderate storms, the total heating rate (Joule + particle) is relatively uniform in the nightside (1800–2400–0600 MLT) [*Baker et al.*, 2004]. Furthermore, the equatorward wind in the nightside thermosphere may not have a large variation with MLT.

[19] The last storm during the 1–4 October period was detected between 0500 and 0700 UT on 4 October 2002.

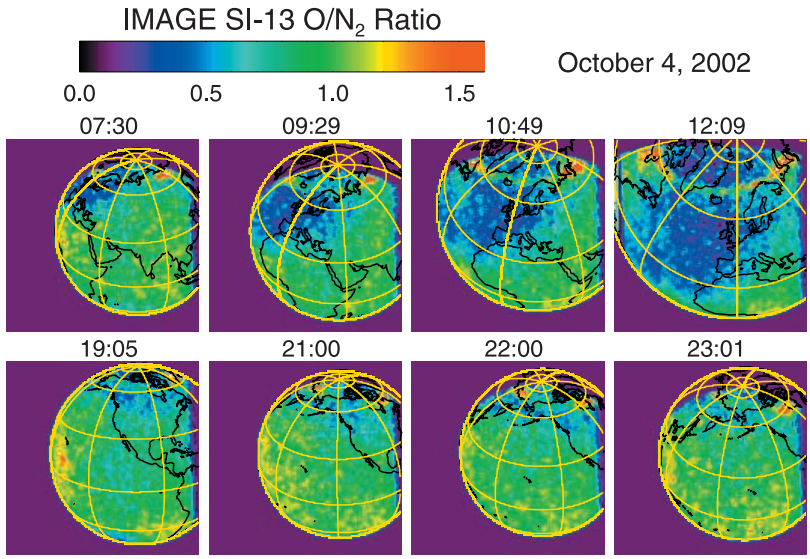

Figure 7. Similar to Figure 4, but for the IMAGE/SI-13 O/N_2 maps between 0730 and 2301 UT, 4 October 2002.

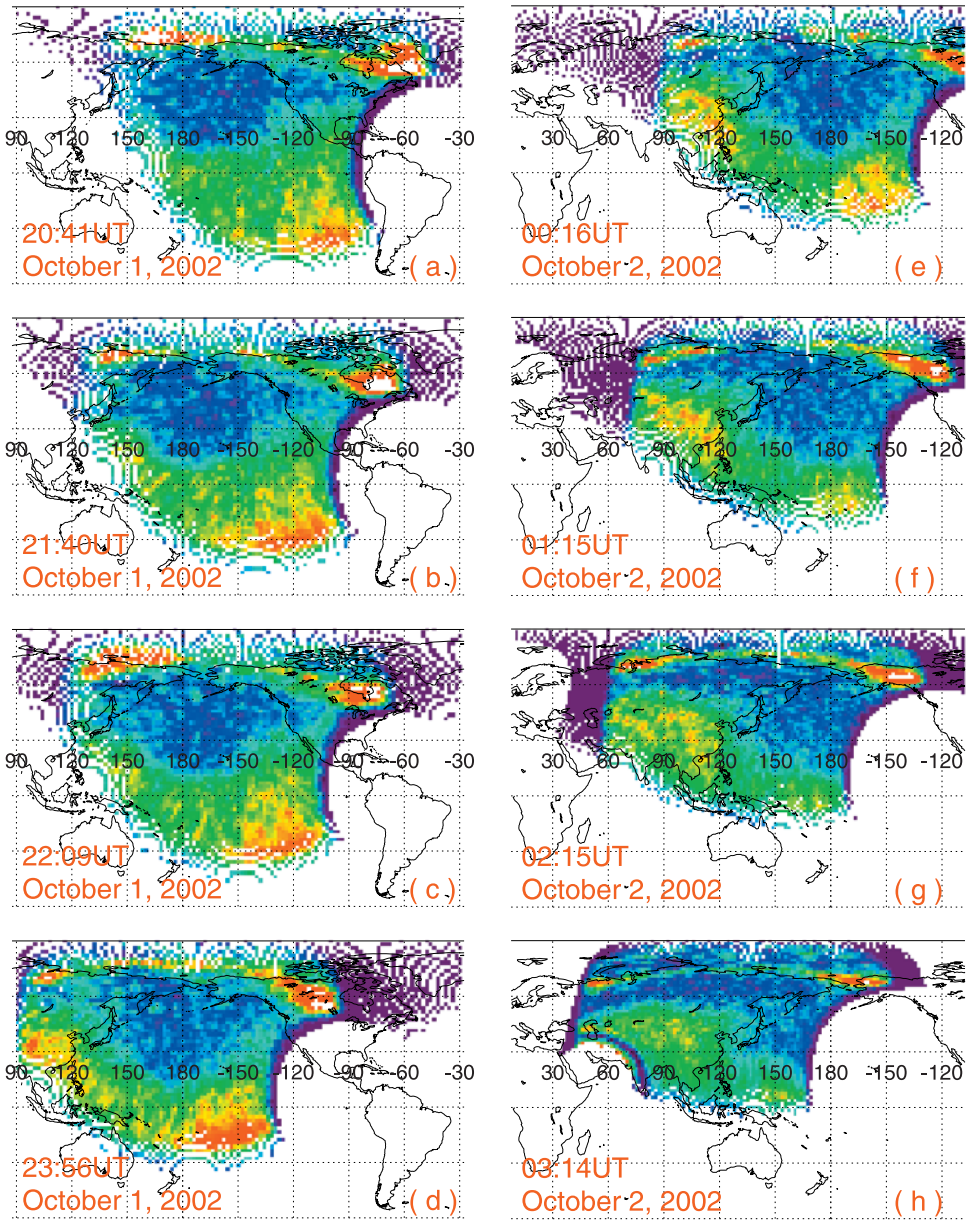

Figure 8. (a)–(d) Remapped IMAGE/SI-13 O/N_2 in a fixed geographic coordinate at 2041, 2140, 2209, and 2356 UT, 1 October 2002. (e)–(h) Remapped IMAGE/SI-13 O/N_2 at 0016, 0115, 0215, and 0314 UT, 2 October 2002. The latitudes are from −60° at the bottom to 90° at the top with a step of 30°.

The Dst was down to −140 nT (see Figure 3). Figure 7 shows that the magnetic storm did cause O/N_2 depletion. The depletion region expanded to latitudes around 20° (see the O/N_2 maps at 1049 and 1209 UT in Figure 7). The Dst started to recover around 1000 UT on 4 October and reached a value around −70 nT by the end of 4 October (see Figure 3). This leads to an undisturbed O/N_2 late on 4 October 2002 at middle and low latitudes (see the images between 1905 and 2301 UT in Figure 7). However, there is still some weak O/N_2 depletion at high (the subauroral) latitudes.

3.2. Corotation of O/N_2 Depletion With the Earth

[20] It is worthwhile to provide direct optical evidence on corotation of the O/N_2 depletion with the Earth even though it has been known for decades [*Park and Meng*, 1976]. Figure 8 shows the SI-13 O/N_2 images at 2041, 2140, 2209, and 2356 UT on 1 October 2002 and 0016, 0115, 0215, and 0314 UT on 2 October 2002 remapped in a fixed geographic coordinate. The horizontal dotted lines are for latitudes from −60° to 90° with a 30° step. O/N_2 depletion in the images is due to the magnetic storm on 1 October 2002. Because of the limited ground coverage in the SI-13 images, the whole depletion region is not seen in each of the images. However, the west-side edge of the depletion between longitudes of 150° and 180° can be identified in each of the images. The edge is located between latitudes of 15° and 30°. The lowest latitude (∼15°) of the depletion around a longitude of 180° can also be found in all the images except the image

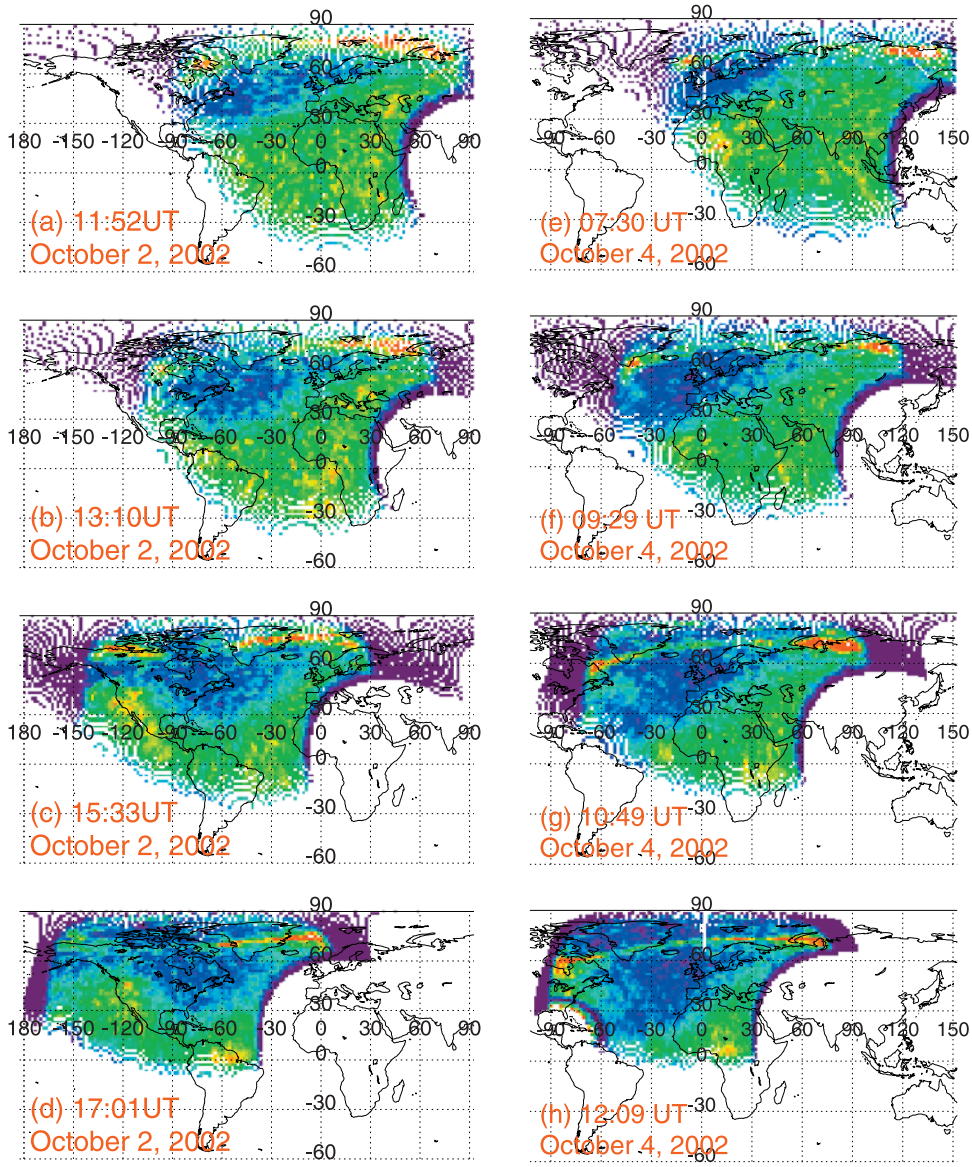

Figure 9. (a)–(d) Remapped IMAGE/SI-13 O/N$_2$ in a fixed geographic coordinate at 1152, 1310, 1533, and 1701 UT, 2 October 2002. (e)–(h) Remapped IMAGE/SI-13 O/N$_2$ at 0730, 0929, 1049, 1209 UT, 4 October 2002. Note images in the left and right columns are due to two independent storms.

in Figure 8h where no O/N$_2$ data are available at the location. Regardless of some temporal changes (~15° in longitude and latitude) in the east edge of the depletion, the depletion region remains fixed in the geographic coordinate. Considering the images cover an interval of 6 hours and 30 min, the Earth rotated 97.5° during the period. This confirms that the depletion region corotates with the Earth.

[21] Figure 9 shows another set of the SI-13 O/N$_2$ images at 1152, 1310, 1533, and 1701 UT on 2 October 2002 and 0730, 0929, 1049, and 1209 UT on 4 October 2002. Owing to possible temporal variation, the depletion in the images on 2 October 2002 appears to shift westward for ~15° in longitude. Note the images (Figures 9a–9d) cover an interval of 5 hours and 9 min (equivalent to rotation angle of 77°). The 15° is only one fifth of the 77°. The depletion in Figures 9e–9h shows that its east-side edge between latitudes 30° and 60° remains between longitudes 0° and 30° over a period of 4 hours and 39 min (~70° of longitude). All these facts also support the corotation idea.

[22] More examples on O/N$_2$ corotation are shown in Figure 10. The O/N$_2$ depletion between 0317 and 0758 UT on 3 October 2002 (Figures 10a–10d) appears to remain roughly at the same location despite the diffused edges and partial view of the depletion. Similar cases are shown in Figures 10e–10h from 1438 to 2131 UT on 3 October 2002. It covers an interval of 6 hours and 53 min (~103° of longitude).

[23] All these examples indicate that the O/N$_2$ depletion indeed corotates with the Earth. The corotation speed may be slightly slower than the Earth's rotational speed. However, the possible temporal variation and errors in the

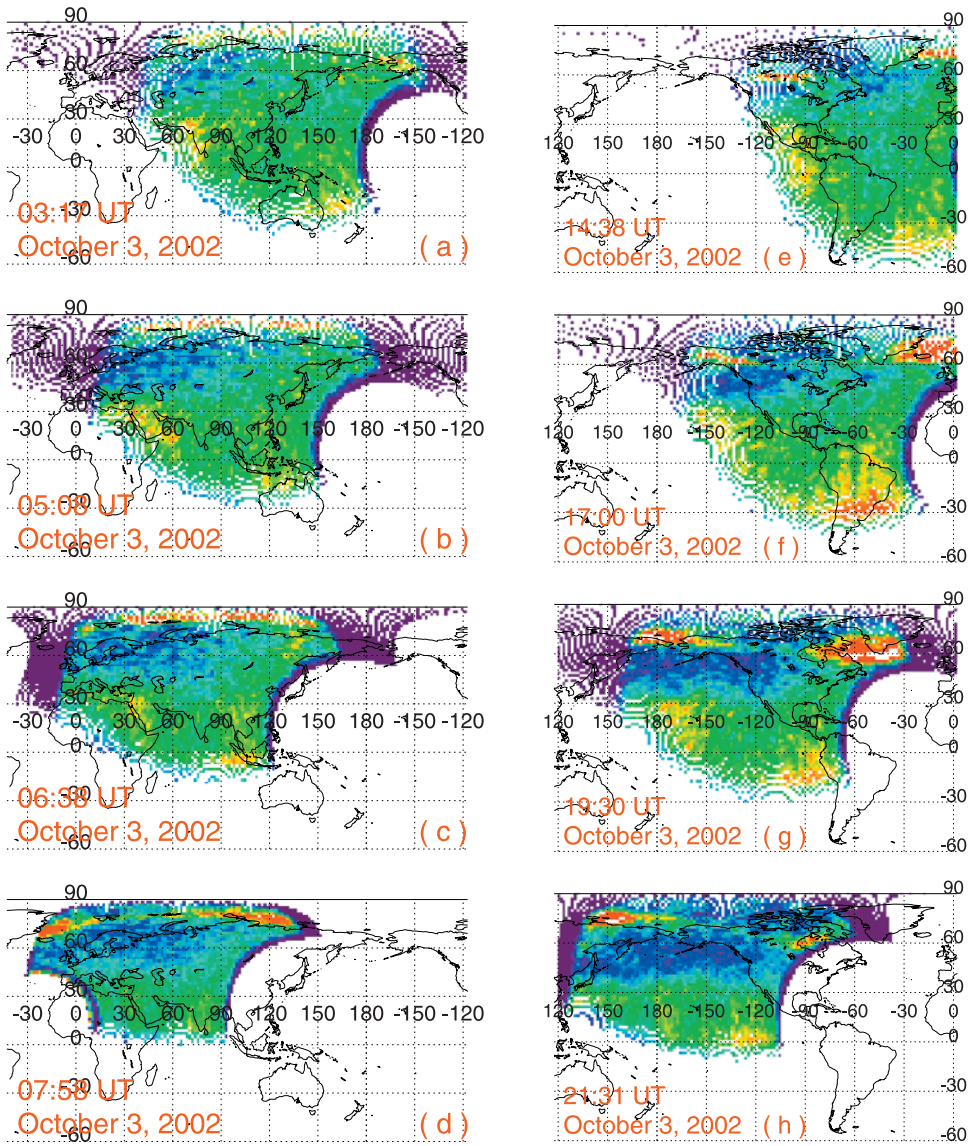

Figure 10. (1)–(h) Remapped IMAGE SI-13 O/N_2 in a fixed geographic coordinate at 0317, 0508, 0638, 0758, 1438, 1700, 1930, and 2131 UT on 3 October 2002.

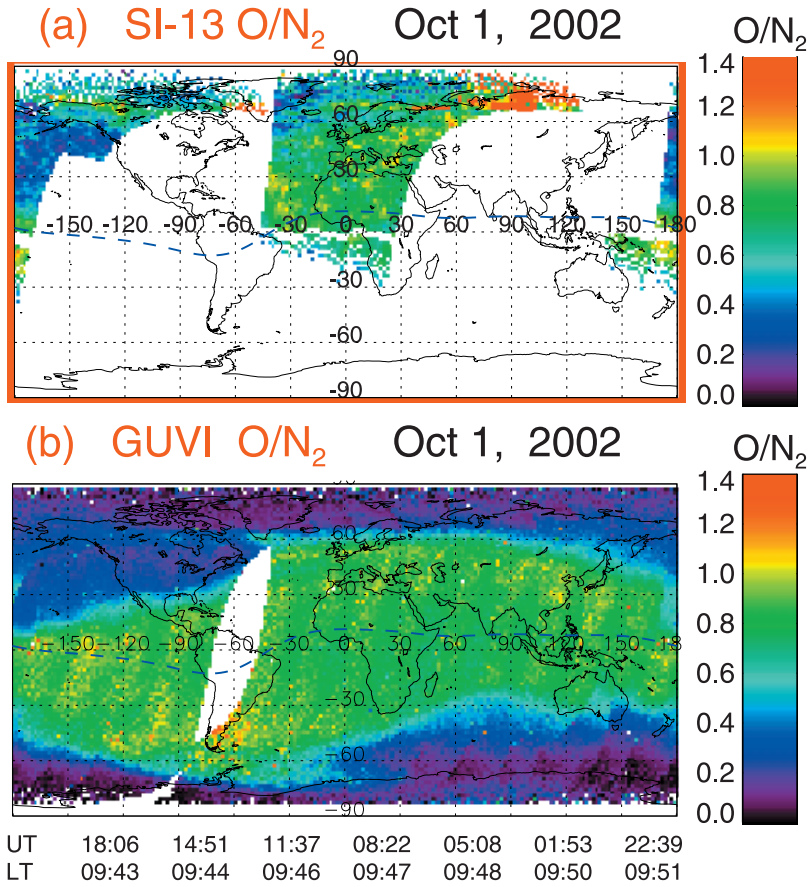

Figure 11. (a) The IMAGE SI-13 O/N_2 map on 1 October 2002. The map was created using the SI-13 O/N_2 values coincident the GUVI pixels (same location ±100 km in both longitude and latitude directions and time ±2 min). The pixels with large values at high latitudes are due to auroral emissions. They should be ignored. (b) The GUVI O/N_2 map on 1 October 2002 from 14 GUVI orbits. The gap is due to missing data for one orbit. The UT and local time (LT) are marked at the bottom. The UT and LT also apply to Figure 11a. The dashed line shows the location of the magnetic equator.

identification of the depletion edge prevent a more accurate analysis.

3.3. Global Comparison of the O/N_2 Obtained From the IMAGE SI-13 and TIMED/GUVI

[24] While the IMAGE SI-13 was monitoring the O/N_2 in the dayside in the Northern Hemisphere during the 4-day period, the TIMED/GUVI was also detecting the O/N_2 in the dayside in both hemispheres but at a relatively fixed local time sector between 0900 and 1000. In order to obtain the O/N_2 values from GUVI data, we used a table from the AURIC runs to rectify the GUVI 135.6 nm and LBHS slant intensities and then normalized them to their equivalent values at a solar zenith angle of 0 degrees. This process removes slant path and SZA effects. Ratios of the rectified and normalized 135.6 nm and LBHS intensities are applied to equation (2) to get the O/N_2 values. We will see that the O/N_2 ratios obtained from two independent instruments (the IMAGE SI-13 and GUVI) show an excellent agreement.

[25] GUVI samples both hemispheres once over each orbit. Figure 11b shows a plot of GUVI O/N_2 map using data from 14 GUVI orbits on 1 October 2002. The O/N_2 are obtained for each super pixel (200 × 200 km). The horizontal and vertical axes are for the longitudes (−180 to 180) and latitudes (−90 to 90), respectively. The gap is due to missing data over one orbit. Note the O/N_2 data are for a nearly fixed local time around 0945. Significant O/N_2 depletion is seen in both the northern and southern polar caps and subauroral latitudes. The depletion region extends to ∼10° of geographic latitude in the Northern Hemisphere (see the left edge in Figure 11b). The O/N_2 remains its quiet time value beyond the depleted regions. The O/N_2 depletion is not symmetric between the two hemispheres in the geographic coordinate.

[26] For a direct comparison, the IMAGE O/N_2 are resampled at each GUVI and IMAGE SI-13 coincident pixel. These coincident O/N_2 data are plotted in Figure 11a in the same format as Figure 11b. Note the IMAGE SI-13 took images in the Northern Hemisphere only. The enhanced values at auroral latitudes in Figure 11a should be ignored as they are due to the auroral contamination. Although we could not find coincident IMAGE data for all the GUVI pixels, the limited coincident data shows a good agreement regarding the O/N_2 from the two instruments on a global scale. Specifically, depletion in the IMAGE O/N_2 at the left edge of Figure 11a also extends down to the equator. Meanwhile, the quiet time O/N_2 values in the center

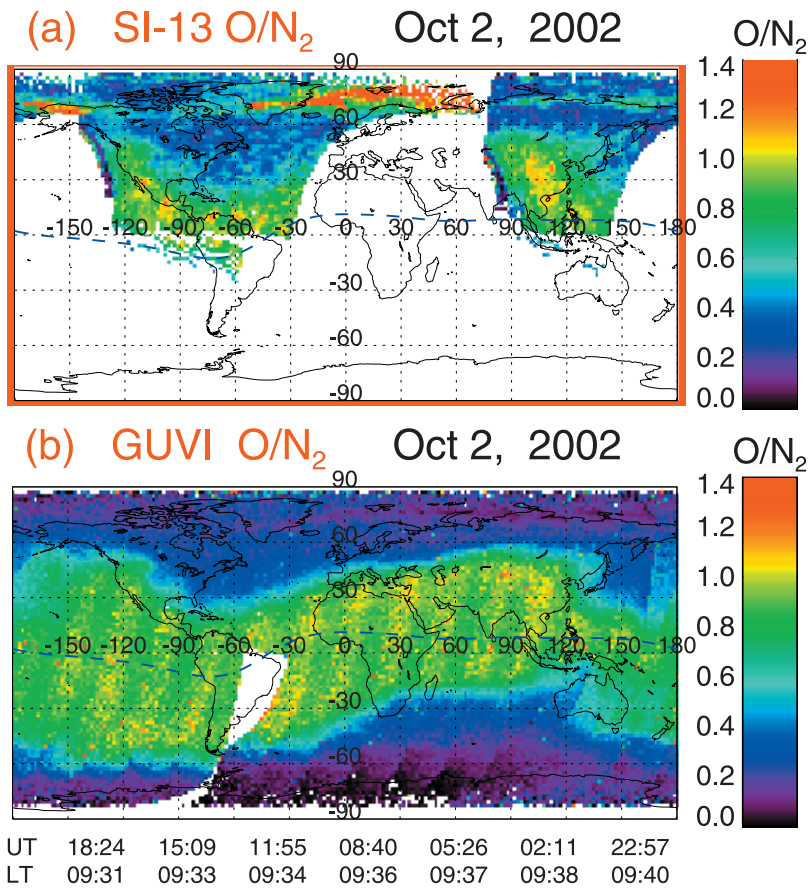

Figure 12. Similar to Figure 11, but for 2 October 2002.

(longitude ~0°) of the GUVI plot (Figure 11b) are reproduced in Figure 11a. Such comparison indicates that O/N_2 from the GUVI and the IMAGE SI-13 have similar morphology and values over a global scale. Detailed comparison will be shown in the next section.

[27] Figure 12, like Figure 11, shows plots of the GUVI and coincident IMAGE O/N_2 on 2 October 2002. By ignoring the auroral contamination, we can see three major features of the O/N_2 depletion in Figure 12a: (1) a large-scale depletion in the North American and Atlantic Ocean sector with its equatorward edge down to latitudes slightly below 30 degrees, (2) relative uniform depletion at sub-auroral latitudes in the east Asian sector, and (3) a shoulder-type depletion region around Japan. Those features are more clearly seen in the GUVI O/N_2 map (see Figure 12b). Furthermore, the O/N_2 depletion in the Southern Hemisphere extended down to −5° around 0211 UT (see the GUVI O/N_2 map in Figure 12b). Again, the O/N_2 from GUVI and IMAGE show a good agreement on the large-scale morphology.

[28] The GUVI O/N_2 plot in Figure 13b (3 October 2002) shows relatively smooth equatorward edges of the depletion regions in both of the hemispheres. There is one exception at the right side of the plot in Figure 13b where the equatorward edge experienced a sudden equatorward shift down to ~40° of latitude. The IMAGE O/N_2 map in Figure 13a shows very similar features in the Northern Hemisphere. When the last magnetic storm occurred on 4 October 2002, GUVI detected a strong depletion with its edge near the equator in the northern Atlantic Ocean (see Figure 14b). The edge gradually moved toward higher latitudes in the east Atlantic Ocean and Europe. This feature was also seen in the IMAGE O/N_2 map in Figure 14a. All these comparisons indicate a good agreement on a large-scale morphology between the GUVI and IMAGE O/N_2.

3.4. Detailed Comparison of O/N_2 Obtained From the IMAGE SI-13 and TIMED/GUVI

[29] For a detailed comparison between the GUVI and IMAGE O/N_2, we selected one GUVI orbit from each of the 4 days (1–4 October 2002) when there were many coincident pixels. Figure 15a shows plots of the GUVI and coincident IMAGE O/N_2 for the GUVI orbit 04408 on 1 October 2002. Ignoring the auroral contamination in the right panel of Figure 15a, the O/N_2 in both of the panels appears to have the same green color or values. However, the color bar in the plot shows the green color may represents the O/N_2 values from 0.7 to 0.9. For a better comparison, we plotted the GUVI and IMAGE O/N_2 together at a few selected meridians or longitudes. Figure 16 shows such kind of plot at longitudes 12.96E, 17.29E, 21.60E, 25.92E, 20.24E, and 34.56E. The large isolated peaks in the IMAGE O/N_2 (green lines) at the high latitudes are due to auroral contamination. The red and green dots show the statistical error levels in the GUVI and SI-13 O/N_2, respectively. The statistical errors are obtained from the count errors in the original GUVI and SI-13 data. The absolute calibration or systematic errors in the SI-13

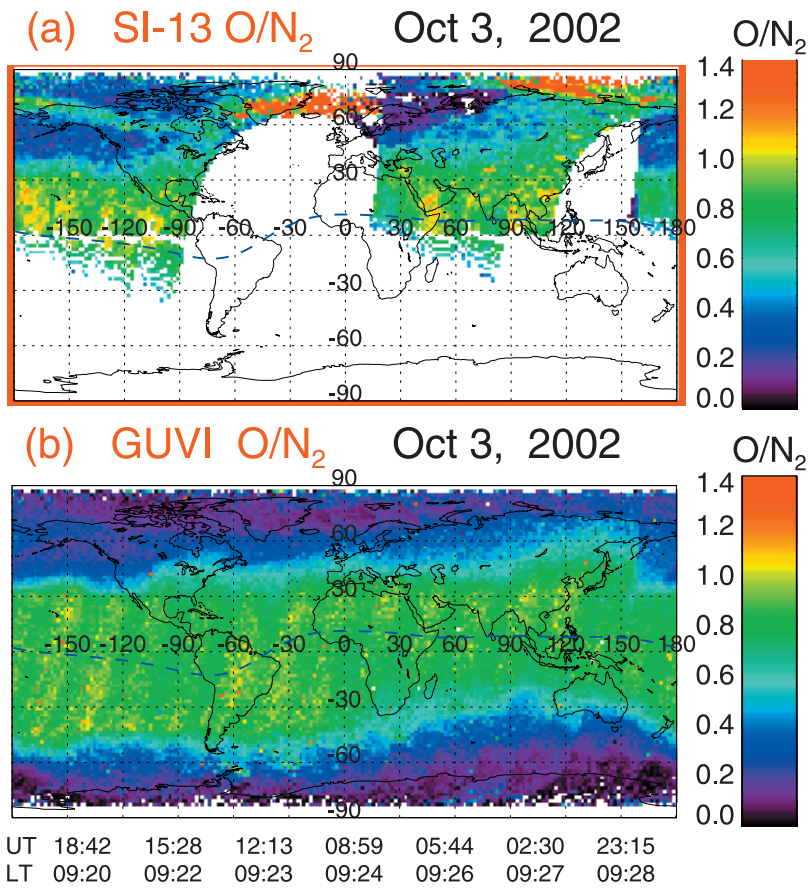

Figure 13. Similar to Figure 11, but for 3 October 2002.

and GUVI data do not affect the estimation of O/N_2, as we used the ratios of the SI-13 intensities and the GUVI 135.6 nm and LBHS intensities. Nevertheless, it is worthwhile to have the information on the calibration errors. The SI-13 preflight absolute calibration was 13 counts/kR/pixel [*Mende et al.*, 2000] and the in-flight calibration was 15.3 counts/kR/pixel [*Frey et al.*, 2003]. This shows confidence that the systematic errors in the absolute calibrations are likely to be less than 20%. The systematic error in the GUVI data is 8%. Both of the GUVI and IMAGE O/N_2 plots show a quiet time value of 0.8 at low latitudes (<40 degrees), slightly higher values at latitudes around 50 degrees, and a steep decrease at latitudes above 60 degrees. Regardless of the auroral contamination, the average statistical errors in the GUVI and SI-13 O/N_2 are ~0.05 and 0.1, respectively. Such error levels are well below the quite time O/N_2 values (~0.84) and depleted O/N_2 values (~0.3) at subauroral latitudes. This confirms that the GUVI O/N_2 agrees very well with the IMAGE O/N_2 and the agreement is statistically significant.

[30] Figure 15b is a plot of the GUVI and IMAGE O/N_2 for GUVI orbit 04428 on 2 October 2002. In addition to the general agreement between the GUVI and IMAGE O/N_2, one small and localized feature, an equatorward penetration at the depletion boundary, is also surprisingly seen in both of the plots. Figure 17, like Figure 16, shows line plots of the GUVI and IMAGE O/N_2 at six different longitudes, 237.60E, 241.92E, 246.24E, 250.56E, 254.88E, and 259.20E on 2 October 2002. The localized feature is visible in Figure 17e around a latitude of 40° and longitude of 254.88°. Figure 17 again shows an excellent and statistically significant agreement between the GUVI and IMAGE O/N_2.

[31] Figure 15c shows a plot of the GUVI and coincident IMAGE O/N_2 for GUVI orbit 04444 on 3 October 2002. Features seen in the GUVI O/N_2 are also clearly seen in the IMAGE O/N_2. Figure 18 again indicates another excellent agreement between the GUVI and IMAGE O/N_2 at different longitudes.

[32] The last example of detailed comparison is shown in Figure 15d for GUVI orbit 04459 on 4 October 2002. The O/N_2 depletion features are again in good agreement between the GUVI and IMAGE O/N_2. However, while GUVI O/N_2 show a slight increase at low and equatorial latitudes, the IMAGE O/N_2 shows a significant localized increase at equatorial latitudes. Such differences can be seen in Figures 19a–19c, as well as at latitudes less than 20° and longitude just below 210°. We found that such an isolated discrepancy is due to the fact that the flat field was incorrect at certain localized pixels in the original SI-13 images. At midlatitudes (between 20 and 60 degrees), the GUVI and IMAGE O/N_2 still show very good agreement (see Figure 19).

4. Discussion

[33] Estimation of the GUVI and IMAGE O/N_2 is based on the same AURIC runs. The IMAGE O/N_2 further

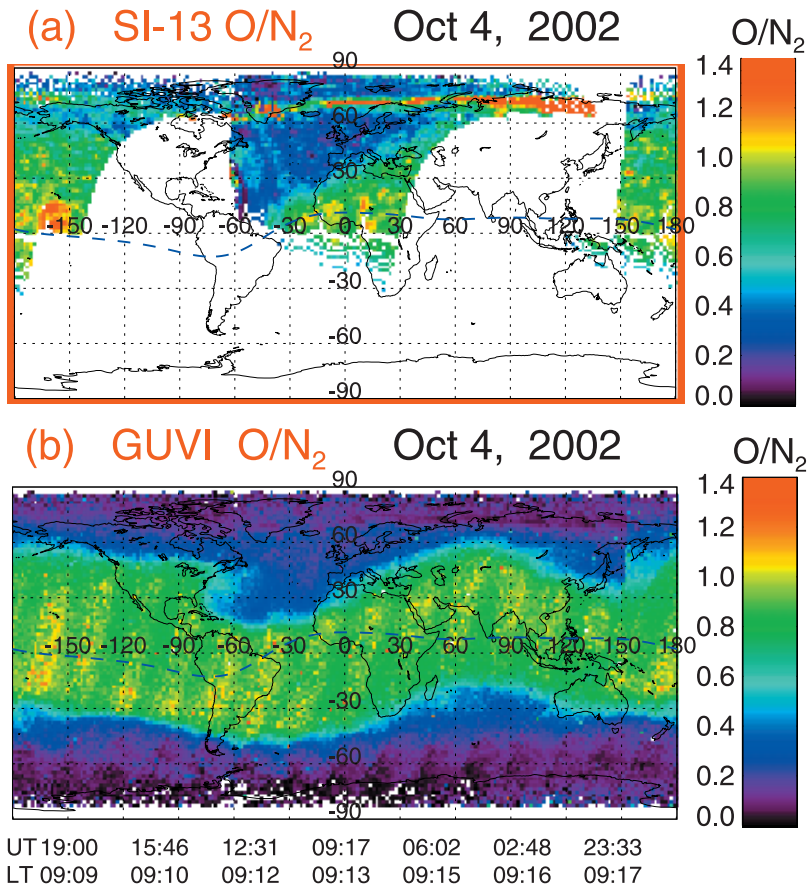

Figure 14. Similar to Figure 11, but for 4 October 2002.

depends on MSIS86 quiet time climatology prior to the storm period. This provides a consistent method to calculate the O/N_2 from the IMAGE SI-13 and GUVI data.

[34] The multiple magnetic storms during the 4-day period (1–4 October 2002) provide a good opportunity to study the response of the thermosphere to the storms. The cases presented in section 3 indicate that each magnetic storm causes a significant O/N_2 depletion. On 1 October 2002 the Dst started a rapid decrease around 0830 UT and reached its minimum level of −185 nT around 1500 UT.

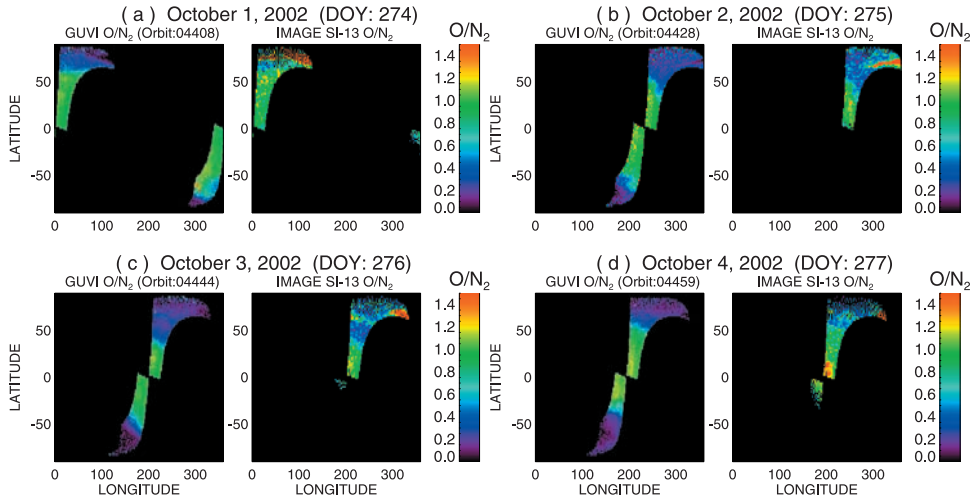

Figure 15. (a)–(d) The GUVI O/N_2 map (left) and the coincident IMAGE SI-13 O/N_2 map for the GUVI orbits 04408 (1 October 2002), 04428 (2 October 2002), 04444 (3 October 2002), and 04459 (4 October 2002), respectively. The large IMAGE SI-13 O/N_2 values at the high latitudes are again due to the auroral emissions.

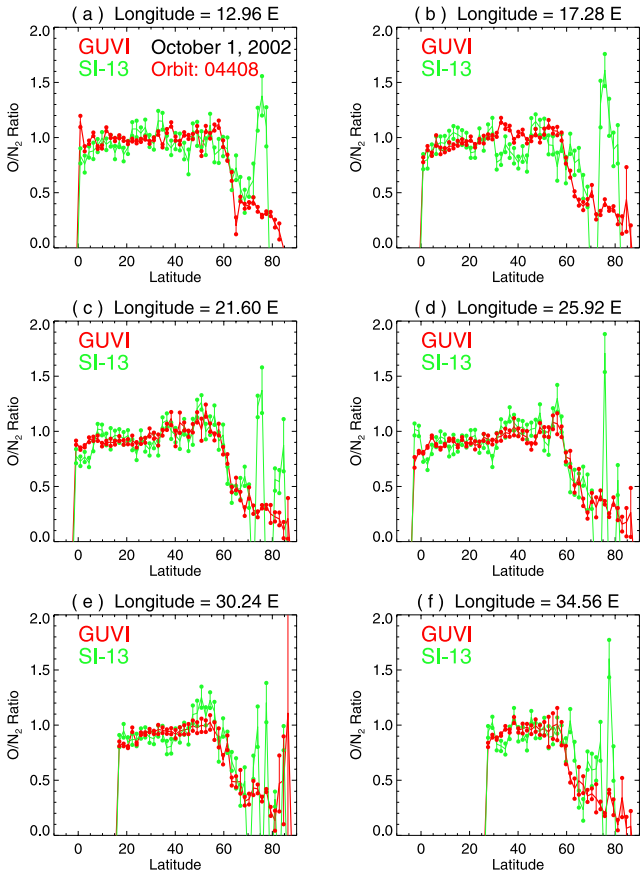

Figure 16. (a)–(f) Six GUVI and SI-13 O/N_2 plots versus latitudes at six different longitudes for the GUVI orbit 04408, 1 October 2002 (see Figure 15). The large SI-13 O/N_2 values at latitudes above 70° are due to auroral emissions. Error bars are marked by the dots.

The O/N_2 depletion was first seen in the polar cap and at subauroral latitudes in the morningside around 1017 UT, ~1.6 hours after the storm started (see Figures 3 and 4). IMAGE started to see the O/N_2 depletion down to low latitudes (~15°) in the morningside ~5 hours after the Dst reached −185 nT around 1500 UT (see the plot at 2041 UT in Figure 4). The depletion reached latitudes of 10° by 2356 UT. Meanwhile, it is evident that the depletion region generally corotated with the Earth (see Figure 8). A 9-hour delay (1500 to 2356 UT) also supports the corotation if we assume the greatest heating occurred around the midnight sector of the auroral oval. On the other hand, the depletion at subauroral latitudes is first seen in the morningside with a short delay (1.6 hours) after the start of a magnetic storm, supporting the prediction by *Immel et al.* [2001] that O/N_2 depletion can be seen in the morning sector ~2 hours after a magnetic storm starts. This suggests that the depletion at subauroral latitudes observed shortly after a magnetic storm is due to Joule and particle heating in the nearby auroral oval, while the low-latitude penetrating depletion observed with a few hour delay after a magnetic storm is due to the intense Joule and particle heating and transport around the nightside auroral oval.

[35] An interesting O/N_2 depletion case occurred on 3 October 2003 when the Dst recovered to −70 nT in the early hours of the day. However, there was a magnetic storm due to a 1-hour duration of southward IMF (Kp was up to 6 between 0000 and 0300 UT). This storm caused a weak depletion with a diffused edge around 45° latitude, though the edge could not be easily identified like other depletions occurring on 1, 2, and 4 October 2002.

[36] It is interesting to note that the minimum O/N_2 at 60 and 70 degrees was down to 0.2 and 0.1, respectively (see GUVI O/N_2 curves in Figures 17, 19, 21, and 23). Such O/N_2 values are only ~24% and 12% of the quiet time O/N_2 (0.84) at lower latitudes.

[37] While the IMAGE SI-13 was monitoring dayglow emissions only in the Northern Hemisphere, the GUVI detected O/N_2 depletion in both of the hemispheres. The depletion is not symmetric in the geographic coordinates at a given local time (see Figures 11 through 14). This is due to possible differences in heating and convection induced winds.

[38] In addition to the features in the O/N_2 depletion, the IMAGE SI-13 and GUVI O/N_2 agree very well with each other on both global (see Figures 11 through 14) and local scales (see Figures 16 through 19). The statistical error levels in Figures 16–19 are well below the O/N_2 values, indicating the agreement is statistically significant. Such an excellent agreement indicates that both of the instruments performed very well. In section 3.2, it was demonstrated that the O/N_2 depletion corotates with the Earth. This indicates that GUVI O/N_2 data at a relatively fixed local

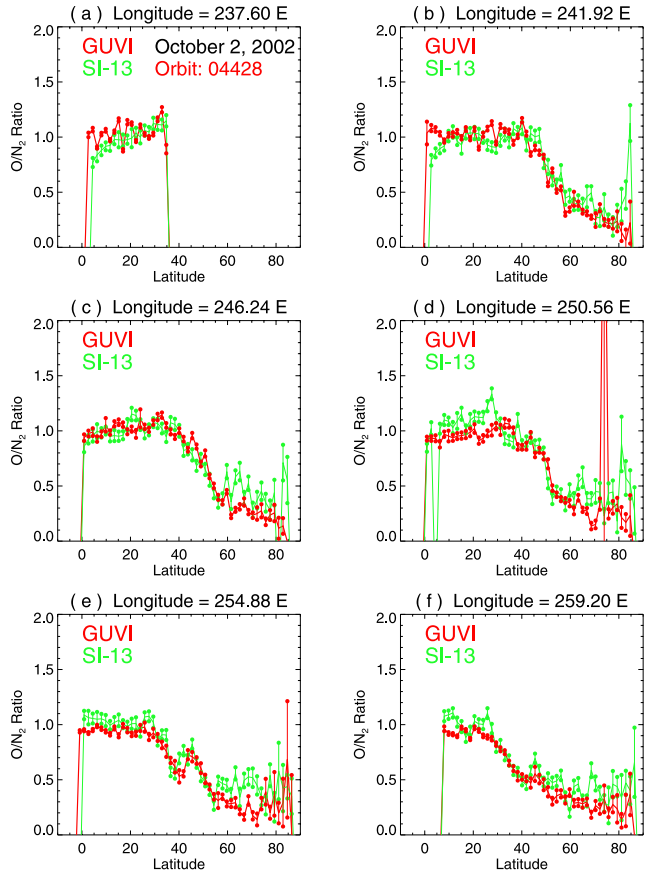

Figure 17. Similar to Figure 16, but for the GUVI orbit 04428, 2 October 2002.

time could be used to a snapshot of the global (both Northern and Southern Hemispheres) O/N_2 map. Both of the IMAGE SI-13 and GUVI O/N_2 maps also provide a good opportunity for future modeling efforts.

5. Summary

[39] The limited study on the O/N_2 changes due to the magnetic storms on 1–4 October 2002 has revealed some interesting features of the O/N_2 depletion and provided a cross check on performance of the SI-13 and GUVI instruments.

[40] 1. Each storm in the 4-day period (1–4 October 2002) caused significant O/N_2 depletion in both the Northern (GUVI and the IMAGE SI-13 data) and the Southern (GUVI data) Hemispheres. The lowest latitudes that the depletions reached are 10° and −5° in the Northern and Southern Hemispheres, respectively.

[41] 2. The simultaneous observations indicate an excellent and statistically significant agreement between the O/N_2 values obtained from two independent instruments, the IMAGE SI-13 and TIMED/GUVI, on both global and local scales.

[42] 3. The IMAGE SI-13 O/N_2 maps provide direct optical evidence that the O/N_2 depletion region corotates with the Earth.

[43] For a better understanding of the atmospheric O/N_2 changes, more IMAGE and GUVI coincident cases in different seasons will be investigated. We also plan to determine total Joule and particle heating rate from the GUVI and IMAGE SI-13 images, electric field data from SuperDarn radar [*Baker et al.*, 2004], and establish an empirical model of the O/N_2 depletion versus the heating rate and solar wind/IMF conditions. This will be very useful for the nowcasting and forecasting of space weather.

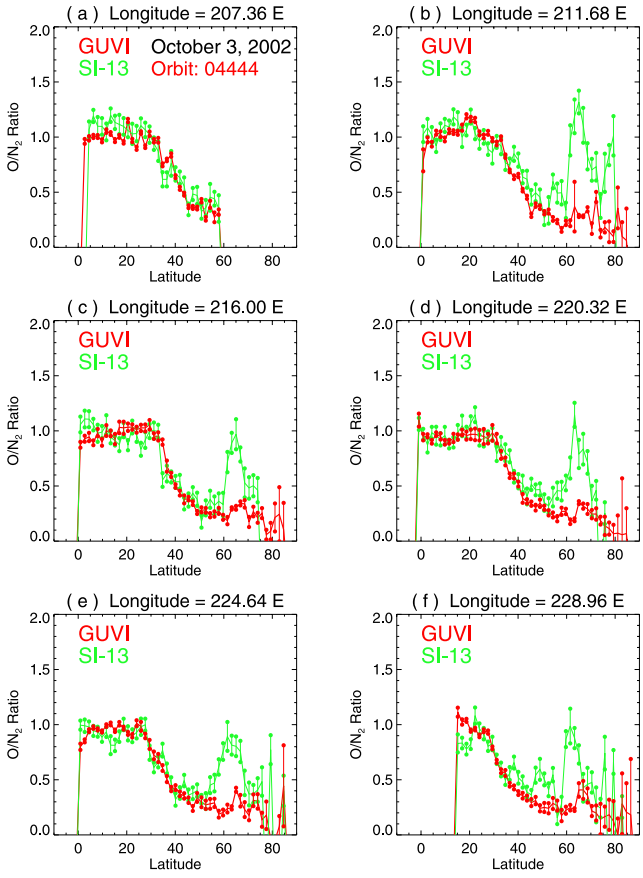

Figure 18. Similar to Figure 16, but for the GUVI orbit 04444, 3 October 2002.

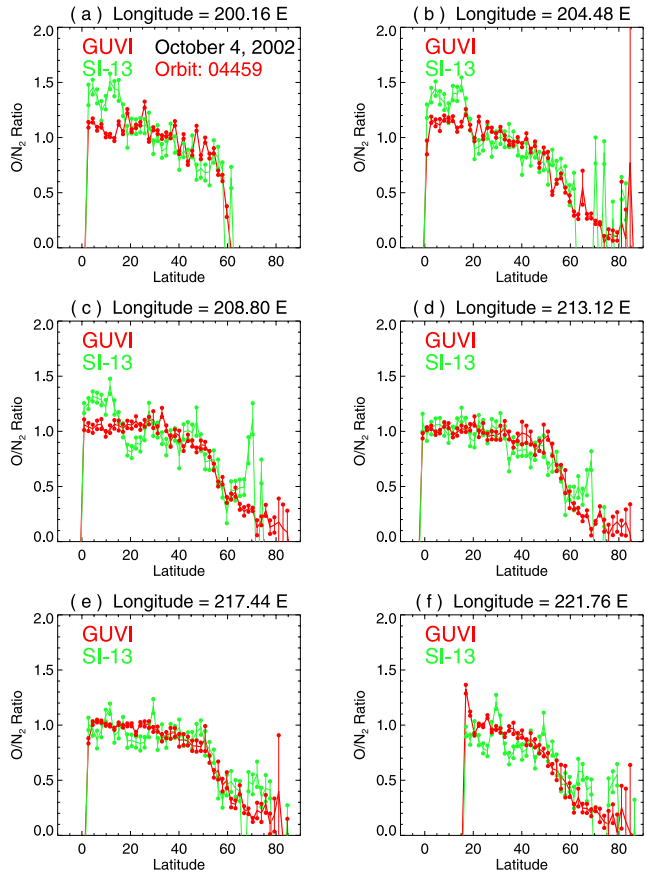

Figure 19. Similar to Figure 16, but for the GUVI orbit 04459, 4 October 2002.

[44] **Acknowledgments.** We are grateful to Doug Strickland for the AURIC code. The Dst and Kp data are obtained from World Data Center 2 at Kyoto (http://swdcdb.kugi.kyoto-u.ac.jp/dstdir/index.html).

[45] Arthur Richmond thanks the reviewers for their assistance in evaluating this paper.

References

Appleton, E. V., and L. J. Ingram (1935), Magnetic storms and upper atmospheric ionization, *Nature*, *136*, 548.

Baker, J. B. H., Y. Zhang, R. A. Greenwald, L. J. Paxton, and D. Morrison (2004), Height-integrated Joule and auroral particle heating in the nightside high-latitude thermosphere, *Geophys. Res. Lett.*, *31*, L09807, doi:10.1029/2004GL019535.

Buonsanto, M. J. (1999), Ionospheric storms—A review, *Space Sci. Rev.*, *88*, 563.

Burns, A. G., T. L. Killen, and R. G. Roble (1989), Causes of changes in the composition calculated using a thermospheric general circulation model, *J. Geophys. Res.*, *94*, 3670.

Christensen, A. B., et al. (1994), The Global Ultraviolet Imager (GUVI) for the NASA TIMED mission, *Proc. SPIE Int. Soc. Opt. Eng.*, *2266*, 451.

Christensen, A. B., et al. (2003), Initial observations with the Global Ultraviolet Imager (GUVI) in the NASA TIMED satellite mission, *J. Geophys. Res.*, *108*(A12), 1451, doi:10.1029/2003JA009918.

Craven, J. D., A. C. Nicholas, L. A. Frank, and D. J. Strickland (1994), Variations in FUV dayglow brightness following intense auroral activity, *Geophys Res. Lett.*, *21*, 2793.

Duncan, R. A. (1969), F-region seasonal and magnetic storm behavior, *J. Atmos. Terr. Phys.*, *31*, 59.

Eastes, R. W. (2000), Modeling the N_2 Layman-Birge-Hopfield bands in the dayglow: Including radiative and collisional cascading between the singlet states, *J. Geophys. Res.*, *105*, 18,557.

Evans, J. S., D. J. Strickland, and R. E. Huffman (1995), Satellite remote sensing of thermospheric O/N_2 and solar EUV: 2. Data analysis, *J. Geophys. Res.*, *100*, 12,227.

Frey, H. U., T. J. Immel, S. B. Mende, J.-C. Gerard, B. Hubert, S. Habraken, J. Spann, G. R. Gladstone, D. V. Bisikalo, and V. I. Sheamatovich (2003), Summary of quantitative interpretation of IMAGE far ultraviolet auroral data, *Space Sci. Rev.*, in press.

Fuller-Rowell, T. J., M. V. Codrescu, H. Rishbeth, R. J. Moffet, and S. Quegan (1996), On the seasonal response of the thermosphere and ionosphere to geomagnetic storms, *J. Geophys. Res.*, *101*, 2343.

Hays, P. B., R. A. Jones, and M. H. Rees (1973), Auroral heating and the composition of the neutral atmosphere, *Planet. Space Sci.*, *21*, 559.

Immel, T. J., J. D. Craven, and L. A. Frank (1997), Influence of IMF By on large-scale decreases of O column density at middle latitudes, *J. Atmos. Terr. Phys.*, *59*, 725.

Immel, T. J., J. D. Craven, and A. C. Nicholas (2000), An empirical model of the OI FUV dayglow from DE-1 images, *J. Atmos. Sol. Terr. Phys.*, *62*, 47.

Immel, T. J., G. Crowley, J. D. Craven, and R. G. Roble (2001), Dayside enhancement of thermospheric O/N_2 following magnetic storm onset, *J. Geophys. Res.*, *106*, 15,471.

Mayr, H. G., and H. Volland (1972), Magnetic storm effects in the neutral composition, *Planet. Space Sci.*, *20*, 379.

Mayr, H. G., I. Harris, and N. W. Spencer (1978), Some properties of upper atmosphere dynamics, *Rev. Geophys.*, *16*, 539.

Mende, S. B., et al. (2000), Far ultraviolet imaging from the IMAGE spacecraft: 3. Spectral imaging of Lyman alpha and OI 135.6 nm, *Space Sci. Rev.*, *91*, 287.

Nicholas, A. C., J. D. Craven, and L. A. Frank (1997), A survey of large-scale variations in thermospheric oxygen column density with magnetic activity as inferred from observations of the FUV dayglow, *J. Geophys. Res.*, *102*, 510–4493.

Park, C. G., and C.-I. Meng (1976), Aftereffects of isolated magnetospheric substorm activity on the midlatitude ionosphere: Localized depressions in *F* layer electron densities, *J. Geophys. Res.*, *81*, 4571.

Paxton, L. J., and C.-I. Meng (1999), Auroral imaging and space-based optical remote sensing, *Johns Hopkins APL Tech. Dig.*, *20*, 556.

Paxton, L. J., et al. (1992), SSUSI: Horizon-to-horizon and limb viewing spectrographic imager for remote sensing of environmental parameters, *Proc. SPIE Int. Soc. Opt. Eng.*, *1764*, 161.

Paxton, L. J., et al. (1999), Global ultraviolet imager (GUVI): Measuring composition and energy inputs for the NASA Thermosphere Ionosphere Mesosphere Energetics and Dynamics (TIMED) mission, *SPIE Opt. Spectrosc. Tech. Instrum. Atmos. Space Res. III*, *3756*, 265–276.

Prölss, G. W. (1980), Magnetic storm associated perturbations of the upper atmosphere: Recent results obtained by satellite-borne gas analyzers, *Rev. Geophys.*, *18*, 183.

Prölss, G. W. (1997), Magnetic storm associated perturbations of the upper atmosphere, in *Magnetic Storms*, *Geophys. Monogr. Ser.*, vol. 98, edited by B. T. Tsurutani et al., pp. 227, AGU, Washington, D. C.

Prölss, G. W., and J. D. Craven (1998), Perturbations of the FUV dayglow and ionospheric storm effects, *Adv. Space Sci.*, *22*, 129.

Prölss, G. W., M. Moemer, and J. W. Slowey (1988), Dissipation of solar wind energy in the Earth's upper thermosphere: The geomagnetic activity effect. CIRA 1986, *Adv. Space Res.*, *8*(5–6), 215.

Schunk, R. W., and J. J. Sojka (1996), Ionosphere-thermosphere space weather issues, *J. Atmos. Terr. Phys.*, *58*, 1527.

Seaton, M. J. (1956), A possible explanation of the drop in F-region critical densities accompanying major ionospheric storms, *J. Atmos. Terr. Phys.*, *8*, 122.

Strickland, D. J., J. S. Evans, and L. Paxton (1995), Satellite remote sensing of thermospheric O/N_2 and solar EUV: 1. Theory, *J. Geophys. Res.*, *100*, 12,217.

Strickland, D. J., J. Bishop, J. S. Evans, T. Majeed, P. M. Shen, R. J. Cox, R. Link, and R. E. Huffman (1999), Atmospheric Ultraviolet Radiance Integrated Code (AURIC): Theory, software architecture, inputs, and selected results, *J. Quant. Spectrosc. Radiat. Transfer*, *62*, 689.

Strickland, D. J., R. E. Daniell, and J. D. Craven (2001), Negative ionospheric storm coincident with DE-1 observed thermospheric disturbance on October 14, 1981, *J. Geophys. Res.*, *106*, 21,049.

Strickland, D. J., R. R. Meier, R. L. Walterscheid, J. D. Craven, A. B. Christensen, L. J. Paxton, D. Morrison, and G. Crowley (2004), Quiet time seasonal behavior of the thermosphere seen in the far ultraviolet dayglow, *J. Geophys. Res.*, *109*, A01302, doi:10.1029/2003JA010220.

Zhang, Y., L. J. Paxton, H. Kil, C.-I. Meng, S. B. Mende, H. U. Frey, and T. J. Immel (2003), Negative ionospheric storms seen by the IMAGE FUV instrument, *J. Geophys. Res.*, *108*(A9), 1343, doi:10.1029/2002JA009797.

T. J. Immel and S. B. Mende, Space Sciences Laboratory, University of California, Berkeley, CA 94720, USA.

H. Kil, C.-I. Meng, D. Morrison, L. J. Paxton, B. Wolven, and Y. Zhang, Johns Hopkins University Applied Physics Laboratory, Laurel, MD 20723, USA. (yongliang.zhang@jhuapl.edu)